CHEMISTRY
A EUROPEAN JOURNAL

DOI: 10.1002/chem.200901954

Synthesis of Highly Efficient Ag@AgCl Plasmonic Photocatalysts with Various Structures

Peng Wang,[a] Baibiao Huang,*[a] Zaizhu Lou,[a] Xiaoyang Zhang,[a] Xiaoyan Qin,[a] Ying Dai,[b] Zhaoke Zheng,[a] and Xiaoning Wang[a]

Abstract: By means of a simple ion-exchange process (using different precursors) and a light-induced chemical reduction reaction, highly efficient Ag@AgCl plasmonic photocatalysts with various self-assembled structures—including microrods, irregular balls, and hollow spheres—have been fabricated. All the obtained Ag@AgCl catalysts were characterized by means of X-ray diffraction, X-ray photoelectron spectroscopy, scanning electron microscopy, and UV-visible diffuse reflectance spectroscopy. The effect of the different morphologies on the properties of the photocatalysts was studied. The average content of elemental Ag in Ag@AgCl was found to be about 3.2 mol%. All the catalysts show strong absorption in the visible-light region. The obtained Ag@AgCl samples exhibit enhanced photocatalytic activity for the degradation of organic contaminants under visible-light irradiation. The stability of the plasmonic photocatalysts was also investigated in detail.

Keywords: heterogeneous catalysis · nanostructures · photocatalysts · photochemistry · silver

Introduction

The precise control of the shapes and structures of inorganic nanoparticles has received great attention owing to their fascinating morphology-dependent chemical, optical, and catalytic properties.[1–4] The assembly of nanoparticles into functional architectures has become increasingly important in the design of novel sensors, circuits, photocatalysts, and devices on the nano- and microscales.[5–8] As a result, remarkable research progress has been accomplished in the past few decades on the synthesis, characterization, and applications of many metallic and semiconducting structures of various architectures.[9–11] Yu et al. successfully fabricated $WO_3 \cdot {}^1/_3 H_2O$ hollow microspheres with hierarchically porous wall structures by means of a one-pot hydrothermal method at 80 °C; these microspheres were more catalytically active due to their increased surface area.[12] Polshettiwar et al. developed a convenient synthetic protocol for metal oxides with 3D nanostructures under microwave irradiation conditions. The metal oxides self-assembled into octahedra, spheres, triangular rods, pine, and hexagonal snowflakelike three-dimensional morphologies, and the pine-structured iron oxides have been widely used as a novel support for various catalytic organic transformations.[13] Ye and co-workers synthesized the hierarchical WO_3 hollow shells—dendrites, spheres, and dumbbells—by simply calcining acid-treated $PbWO_4$ and $SrWO_4$ precursors at 500 °C for 2 h. Compared with commercial WO_3 particles, all the obtained hollow shells showed enhanced photocatalytic activities for the degradation of organic contaminants under visible-light irradiation.[14] However, it is still a challenge for chemists and materials scientists to fabricate novel self-assembling functional architectures.[15]

The development of visible-light-driven photocatalysts has been an attractive research field due to ambitions of water splitting, pollutant destruction, and bacterial disinfection.[16,17] Most research has been concentrated on anatase (TiO_2), which is photostable, nontoxic, cheap, and active. Due to its large band gap of 3.2 eV, UV light ($\lambda < 400$ nm) is necessary to generate the electron–hole pairs, thus restricting its absorption of solar energy (about 4% of the total energy). Thus, several attempts have been made to overcome this barrier, including phase and morphological control, doping, surface sensitization, composite photocatalysts,

[a] P. Wang, Prof. Dr. B. Huang, Z. Lou, X. Zhang, X. Qin, Z. Zheng, X. Wang
State Key Laboratory of Crystal Materials
Shandong University, Jinan 250100 (China)
E-mail: bbhuang@sdu.edu.cn

[b] Prof. Dr. Y. Dai
School of Physics
Shandong University, Jinan 250100 (China)

heterojunction photocatalysts, and plasmonic photocatalysts.[18–20] Among them, the plasmonic photocatalysts are one of the most promising approaches because of their outstanding performance in photocatalytic processes. The plasmonic photocatalyst combines the plasmon resonance of noble-metal nanoparticles with a semiconductor catalyst. Noble-metal nanoparticles (NPs) show strong visible-light absorption because of size- and shape-dependent plasmon resonance, which accelerates the separation process of the photogenerated electrons and holes in the semiconductor catalyst. We have demonstrated that the plasmonic photocatalyst Ag@AgCl is efficient and stable under visible light because the Ag nanoparticles strongly absorb visible light, prevent photogenerated electrons from combining with Ag^+ ions, and allow the formation of Cl^0 atoms by combining Cl^- ions with photogenerated holes, and the Cl^0 oxidizes the organic pollution efficiently.[21]

In the present report, we explore a simple ion-exchange method and light-induced chemical reduction reaction for the controlled synthesis of hierarchical Ag@AgCl microstructures including rodlike, irregular ball, and hollow-sphere morphologies. All the samples are assembled from Ag and AgCl nanoparticles. The ion-exchange process is between silver molybdate and hydrochloric acid; the structure of the silver molybdate precursor decides the morphology of Ag@AgCl. The content of the Ag in Ag@AgCl has been determined by X-ray photoelectron spectroscopy. All the obtained Ag@AgCl samples show strong absorption in the visible-light region. It is demonstrated that the morphologies play important roles in the photocatalytic activity. Compared with other Ag@AgCl samples, the Ag@AgCl with a hollow-sphere morphology exhibits superior efficiency in the degradation of organic pollution under visible-light irradiation. The study shows that it is possible to synthesize the highly efficient Ag@AgCl plasmonic photocatalyst by controlling the morphology of the sample.

Results and Discussion

Various structures of Ag@AgCl were synthesized from silver molybdate precursors with similar morphologies. Microrods of silver molybdate, and cubic- and polyhedron-like silver molybdate precursors with abnormal shapes were first prepared by using a microwave-assisted hydrothermal method. The silver molybdate served as the sacrificial template in the fabrication of the structures. The structure and morphology of the precursors played an important role in the morphology of Ag@AgCl.

The crystal structures of the precursors were examined by means of X-ray diffraction (XRD). As shown in Figure 1a, all the peaks can be indexed to the hexagonal phase (space group $P63/m$) of $Ag_{1.028}H_{1.852}Mo_{5.52}O_{18}$ with lattice constants $a=10.60070$ Å and $c=3.72690$ Å (JCPDS card no. 83-1173). The patterns in Figure 1b and c can be indexed to the cubic phase (space group $Fd\bar{3}m$) of Ag_2MoO_4 with lattice constant $a=9.26$ Å (JCPDS card no. 75-250). No characteristic peaks

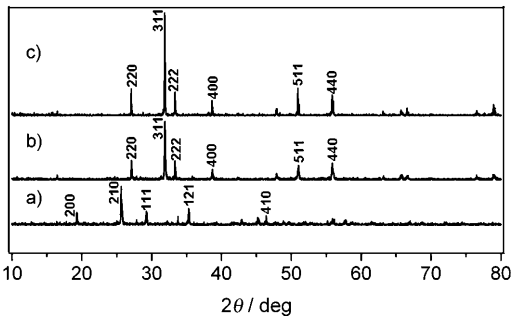

Figure 1. The XRD patterns of the as-prepared precursors. a) $Ag_{1.028}H_{1.852}Mo_{5.52}O_{18}$; b) and c) Ag_2MoO_4.

belonging to other impurities were detected, thus indicating that pure precursors had been synthesized.

After the synthesis of the pure precursors, the ion-exchange process between the precursors and hydrochloric acid resulted in the formation of AgCl with various structures including microrods, irregular balls, and hollow spheres. During the ion-exchange process, the following reaction occurred [Eq. (1)]:

$$Ag_2MoO_4 + HCl \rightarrow AgCl + MoO_3 + H_2O \quad (1)$$

The synthesized MoO_3 was dissolved in an excess amount of HCl, and the AgCl depositions were collected. The AgCl depositions were then put into a solution of methyl orange (MO) dye, which was irradiated with a 300 W Xe arc lamp equipped with an ultraviolet cut-off filter to provide visible light with $\lambda \geq 400$ nm. Then the resulting precipitates, which consisted of silver NPs deposited on AgCl particles, were washed and dried in air. The crystal structures of the Ag@AgCl samples were examined by XRD.

The XRD pattern of the obtained Ag@AgCl products (Figure 2) can be indexed to the cubic phase of Ag with lattice constant $a=4.0861$ Å (JCPDS file: 65-2871) coexisting with the cubic phase of AgCl with lattice constant $a=5.5491$ Å (JCPDS file: 31-1238).

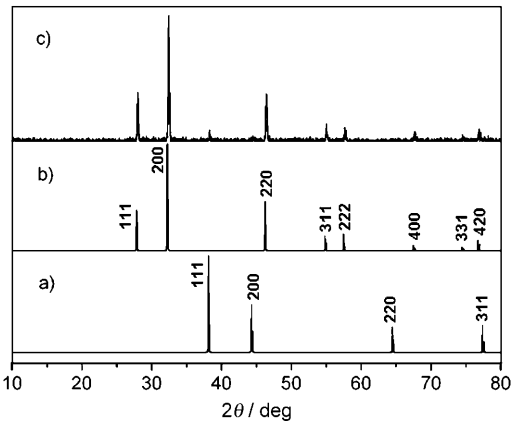

Figure 2. The XRD patterns of a) Ag (JCPDS file: 65-2871), b) AgCl (JCPDS file: 31-1238), and c) Ag@AgCl.

The elemental composition, chemical status, and silver content of Ag@AgCl were further analyzed by means of X-ray photoelectron spectroscopy (XPS). Before the visible-light irradiation, XPS results indicated that Ag@AgCl contained Ag, Cl, and C. The carbon peak is due to the adventitious hydrocarbon from the XPS instrument itself. The Ag and Cl peaks are from the obtained Ag@AgCl samples. The XPS results of Ag@AgCl fabricated from the polyhedron-like Ag_2MoO_4 are shown in Figure 3. The binding energies

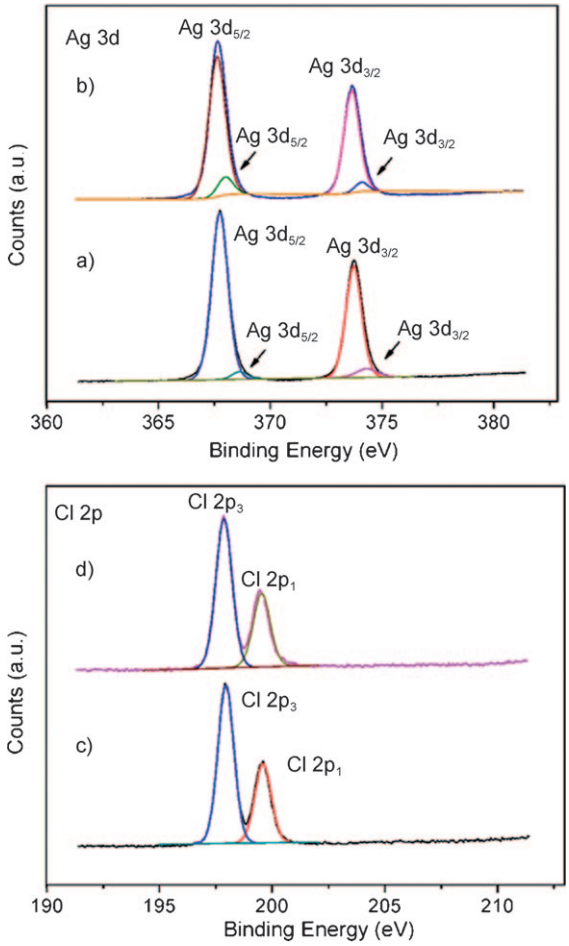

Figure 3. XPS spectra of a) Ag 3d and c) Cl 2p of Ag@AgCl fabricated from the polyhedron-like Ag_2MoO_4; and b) Ag 3d and d) Cl 2p of the corresponding Ag@AgCl used for five consecutive photooxidation experiments with the MO-dye solution under visible-light irradiation.

in the XPS spectra presented here were calibrated with the C 1s peak (284.8 eV). In Figure 3a, the Ag 3d spectra of Ag@AgCl consists of two individual peaks at approximately 373 and approximately 367 eV, which can be attributed to Ag $3d_{3/2}$ and Ag $3d_{5/2}$ binding energies, respectively. The Ag $3d_{3/2}$ and Ag $3d_{5/2}$ peaks can be further divided into two different peaks at 373.74, 374.33 eV and 367.74, 368.64 eV, respectively. According to Zhang et al.,[22] the peaks at 374.33 and 368.64 eV can be attributed to Ag^0, whereas the peaks at 367.74 and 373.74 eV can be attributed to Ag^I (AgCl). The XPS results determined the existence of Ag^0; the calculated surface Ag^0 content of the corresponding samples is 3.46 mol% and the calculated surface Ag^+ content is 48.33 mol%. The spectra of Cl 2p is shown in Figure 3c: the binding energies of Cl $2p_1$ and Cl $2p_3$ are approximately 199.59 and approximately 197.95 eV, respectively, and the calculated surface Cl^- content is 48.23 mol%.

The XPS results of the Ag@AgCl synthesized from the $Ag_{1.028}H_{1.852}Mo_{5.52}O_{18}$ microrod precursor and another Ag_2MoO_4 precursor (not shown here) show that the calculated surface Ag^0 content is 3.15 and 3.05 mol%, the calculated surface Ag^+ content is 48.12 and 47.83 mol%, and the calculated surface Cl^- content is 48.73 and 49.12 mol%, respectively.

The SEM images of the synthesized $Ag_{1.028}H_{1.852}Mo_{5.52}O_{18}$ microrod precursors are shown in Figure 4a and b. The rods are about 40–120 μm in length. Figure 4b shows a typical

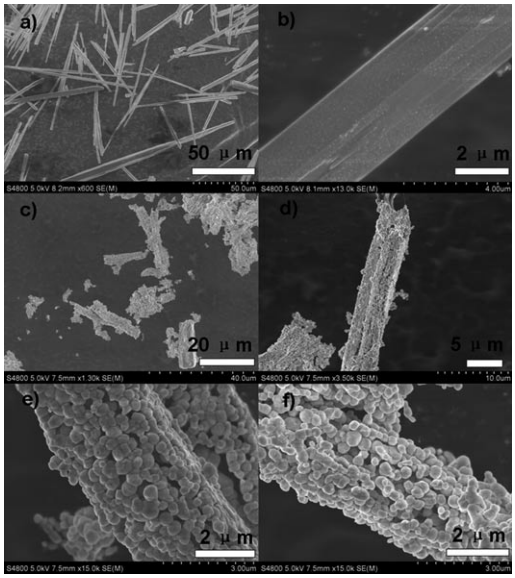

Figure 4. a) and b) SEM images of $Ag_{1.028}H_{1.852}Mo_{5.52}O_{18}$ microrod precursors; c)–f) SEM images of the corresponding Ag@AgCl with different magnifications.

$Ag_{1.028}H_{1.852}Mo_{5.52}O_{18}$ microrod. The diameter of the rod is about 3.3 μm. The SEM images of the corresponding Ag@AgCl product obtained from the $Ag_{1.028}H_{1.852}Mo_{5.52}O_{18}$ microrod precursor are shown in Figure 4c–f. From Figure 4c it can be seen that the length of the Ag@AgCl microrod is shorter than the $Ag_{1.028}H_{1.852}Mo_{5.52}O_{18}$ precursor. The Ag@AgCl microrod tends to aggregate. Figure 4d displays one rod of Ag@AgCl: the length of this rod is about 24 μm and its diameter is about 5.5 μm. Further images (Figure 4e,f) show that the Ag@AgCl microrod is made up of many small nanoparticles. The nanoparticles with diameters of 130–470 nm are composed of Ag nanoparticles and AgCl nanoparticles. It is difficult to observe the Ag and AgCl nanoparticles because the high-energy electron beam can decompose AgCl, thus preventing higher-resolution images from being obtained.

Figure 5a–c show the images of Ag_2MoO_4 with the microrod and cube morphologies. The Ag_2MoO_4 microrods are about 50–220 μm in length and their diameters are about 2–

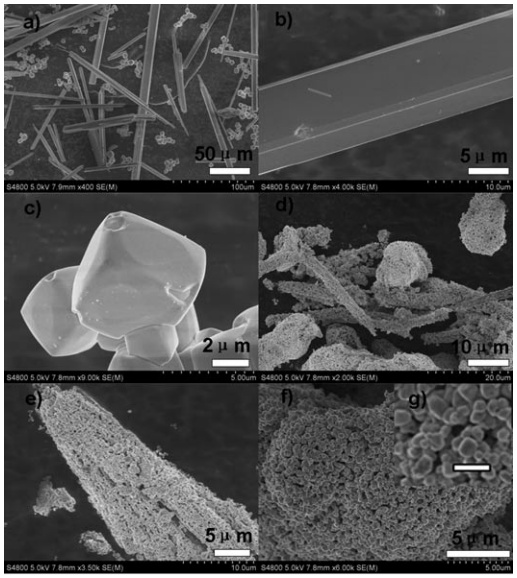

Figure 5. a), b), and c) SEM images of Ag_2MoO_4 microrods and cubes; d) SEM image of the corresponding Ag@AgCl microrod and irregular-ball morphologies; e) SEM image of an Ag@AgCl microrod with different magnifications; f) and g) SEM images of the Ag@AgCl irregular-ball morphology with different magnifications (the bar in Figure 5g is 1 μm).

12 μm. The side length of the Ag_2MoO_4 cubes is 4 μm or so. A single rod and cubelike Ag_2MoO_4 are shown in Figure 5b and c, respectively. The corresponding Ag@AgCl product images are displayed in Figure 5d–g. In Figure 5d–g it can be seen that the small Ag and AgCl nanoparticles assemble into the microrod and irregular ball-like Ag@AgCl. The lengths of the Ag@AgCl microrods are in the range of 10–30 μm, and the diameter of the irregular ball-like Ag@AgCl (Figure 5d) is about 10 μm. In Figure 5g it can be seen that the diameters of the Ag and AgCl nanoparticles are in the range of 110–440 nm.

Figure 6a and b show the SEM images of the obtained polyhedron-like Ag_2MoO_4. As seen from the images, the shape of the Ag_2MoO_4 is irregular, and the Ag_2MoO_4 grains reveal more than four crystal faces. The diameter of the grains is 1.5–10 μm. The representative SEM images of Ag@AgCl achieved from this precursor are shown in Figure 6c–g. Typical SEM images Figure 6c and d indicate that the Ag@AgCl is made up of hollow spheres with a size distribution of 3–14 μm. The high-magnification SEM images (Figure 6e–g) clearly show that the shells of the hollow spheres are composed of many small Ag and AgCl particles with diameters of 83–225 nm. The average wall thickness of the hollow microspheres is about 1.6 μm. The morphology of all the samples was also examined by transmission electron microscopy (TEM, not shown here). The walls of the samples are so thick that good TEM imaging of the hollow

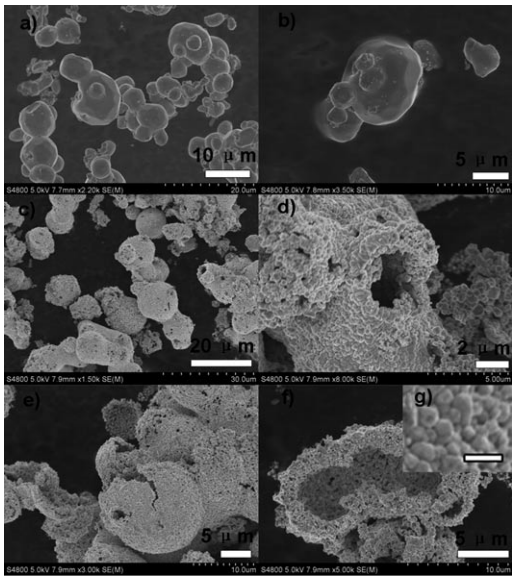

Figure 6. a), b) SEM images of the polyhedron-like Ag_2MoO_4; c)–g) SEM images of the corresponding Ag@AgCl with different magnifications (the bar in Figure 6g is 500 nm).

structures could not be obtained. It should be emphasized that the primary Ag and AgCl nanoparticles aggregate to form fine microstructures, which include the microrods, hollow spheres, and the mixture of microrods and irregular balls. These aggregations are due to the ion-exchange reaction between the hydrochloric acid and silver molybdate. The morphology of the silver molybdate determines the structure of the Ag@AgCl.

The UV-visible diffuse reflectance spectra (Figure 7) of the samples show that all the samples have strong absorption both in the ultraviolet and visible-light regions. The ab-

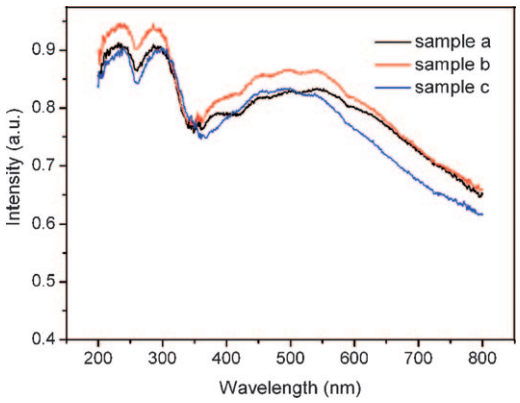

Figure 7. UV/Vis diffuse reflectance spectra of all the obtained Ag@AgCl samples.

sorption at 200–350 nm can be ascribed to the characteristic absorption of the AgCl semiconductor, and the strong absorption in the visible-light region can be attributed to the surface plasmon resonance of silver nanoparticles. Due to the size and the particular surroundings of the silver nano-

particles, the sample exhibits stronger absorption at 450–550 nm. The strong absorption makes the sample use the sunlight more efficiently. For convenience, Ag@AgCl synthesized from the $Ag_{1.028}H_{1.852}Mo_{5.52}O_{18}$ precursor is named sample a; the Ag@AgCl fabricated from Ag_2MoO_4 with microrod and cube morphologies is named sample b; and the Ag@AgCl synthesized from the polyhedron-like Ag_2MoO_4 is named sample c. We can see that the intensities of the visible-light absorption are different, and that sample b displays the highest intensity.

The photooxidation capabilities of the samples were evaluated by measuring the decomposition of methyl orange (MO) dye (with a concentration of 20 mg L^{-1}) over the samples under visible-light irradiation ($\lambda \geq 400$ nm). Figure 8a shows the degradation rate of MO over different photocatalysts. Prior to visible-light irradiation, the MO solution over the catalyst was kept in the dark for 30 min to obtain the equilibrium adsorption state. The concentration of the MO solution slightly decreases while it is kept in the dark; C_0 is the equilibrium concentration of MO at the equilibrium adsorption state, and C is the concentration of MO after visible-light irradiation. A blank experiment in the absence of the photocatalyst but under visible-light irradiation showed that no MO had decomposed. Another blank experiment using sample c as the photocatalyst without irradiation demonstrated that the concentration of MO remained unchanged. The MO solution was decolorized completely by using sample c (hollow spheres) after visible-light irradiation for 40 min (Figure 8a). Provided that the bleaching reaction follows a pseudo-first-order reaction, the rate of the MO-dye decomposition over sample c is estimated to be about 0.05 mg min^{-1}, thus faster than that over N-doped TiO_2 (ca. 0.017 mg min^{-1}).[21] The decompositions over samples a and b were completed in 90 and 70 min of visible-light irradiation, respectively, and the rate of the MO-dye decomposition is estimated to be about 0.0222 and 0.0285 mg min^{-1}, respectively. Samples a–c are therefore more efficient than N-TiO_2. The outstanding photocatalytic activities of photocatalysts a–c for the degradation of pollutants are related to the size of Ag and AgCl, the high adsorption of visible light, and the effective separation of the photogenerated electrons and holes. The good surface contact of the Ag metal particles to the AgCl matrix also plays an important role in enabling the metal–semiconductor heterojunctions to function, thus enhancing the charge transfer, and hence improving the photocatalysis efficiency.

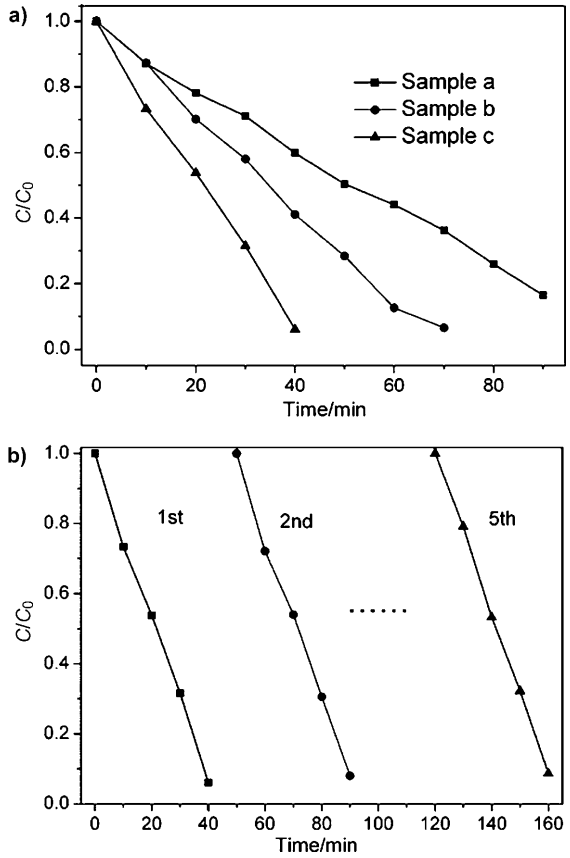

Figure 8. a) Photodecomposition of MO dye in solution (20 mg L^{-1}) over Ag@AgCl (samples a–c) under visible-light irradiation ($\lambda \geq 400$ nm). C is the concentration of MO at time t, and C_0 that in the MO solution immediately after it is kept in the dark to obtain the equilibrium adsorption state. b) The repeated bleaching of MO over recycled sample c under visible light.

Of the Ag@AgCl photocatalysts, sample c has a higher photocatalytic activity for the degradation of MO than samples a or b, despite having similar starting materials. As commonly known, the morphologies of Ag@AgCl nanoparticles have a great influence on their photocatalytic properties. Different morphologies lead to different surface areas, which determine the photocatalytic activity directly. During the MO degradation process, the MO molecules can infiltrate the inside of the Ag@AgCl hierarchical hollow spheres, thus making contact with the inner and outer surface of sample c, and hence improving the photocatalysis efficiency. Whereas with samples a and b, the MO molecules can only make contact with the outer surface of the assembled Ag@AgCl, thus leading to the lower photocatalysis efficiency.

The stability of a photocatalyst is very important for its application. So, as an example, the stability of plasmonic photocatalyst Ag@AgCl (sample c) has been further investigated by recycling it in repeated MO bleaching experiments. As shown in Figure 8b, the MO dye is quickly bleached after every injection of the MO solution, and the Ag@AgCl photocatalyst is stable under repeated application without exhibiting any significant loss of activity.

The XRD pattern and SEM images of sample c at the end of the repeated photocatalytic experiment are almost identical to that of the as-prepared sample c (not shown here). The XPS spectra of sample c used in five consecutive bleaching experiments is shown in Figure 3, and the calculated surface Ag content of the corresponding samples are 3.51 mo %. The change of the Ag content is within the range of the error of the apparatus. Therefore, it should be considered that the Ag@AgCl sample under our experimental con-

ditions is a highly efficient and stable photocatalyst under visible-light irradiation.

As reported in our early work,[21] the stability of the Ag@AgCl plasmonic photocatalyst under visible-light irradiation may be attributed to the fact that the photogenerated electrons in AgCl are absorbed by the silver NPs rather than being transferred to the Ag^+ ions of the AgCl lattice. The localized surface plasmon state of a silver NP lies in the visible region, so absorption of visible light by the Ag@AgCl catalyst takes place at the silver NPs. Given the dipolar character of the surface plasmon state of a silver NP, an absorbed photon would be efficiently separated into an electron and a hole such that an electron is transferred to the surface of the NP farthest away from the Ag/AgCl interface, and a hole to the surface of the AgCl particle bearing the NP. The holes are transferred to the AgCl surface corresponding to the oxidation of Cl^- ions to Cl^0 atoms, which should be able to oxidize MO dye and hence be reduced to chloride ions again. In general, photogenerated electrons are expected to be trapped by O_2 in the solution to form superoxide ions (O_2^-) and other reactive oxygen species.[23]

Conclusion

In summary, various self-assembled structures—including microrods, irregular balls, and hollow spheres—of the highly efficient plasmonic photocatalyst Ag@AgCl have been fabricated by means of an ion-exchange process (between different $Ag_{1.028}H_{1.852}Mo_{5.52}O_{18}$ and Ag_2MoO_4 precursors and hydrochloric acid) and a light-induced chemical reduction reaction. All the obtained Ag@AgCl samples were assembled from small Ag and AgCl nanoparticles. The Ag@AgCl catalysts exhibit strong adsorption in the visible-light region for the plasmon resonance of Ag nanoparticles, and the Ag@AgCl hollow spheres show a higher photocatalytic activity in the degradation of MO than other samples. The XRD pattern and XPS spectra of the Ag@AgCl samples prove their stability. With their strong adsorption in the visible-light region, high photocatalytic activity, and high photostability, the plasmonic photocatalysts are promising candidates for the development of highly efficient and stable visible-light photocatalysts, sensors, and solar cells.

Experimental Section

Materials: Silver nitrate was purchased from Statepharm Chemical Reagent Co. Ltd. (Shanghai) and hydrochloric acid was purchased from Kangde Chemical Reagent Co. Ltd. (Shandong). Sodium molybdate and sodium hydroxide were purchased from Kemel Chemical Reagent Co. Ltd. (Tianjing). All the reagents were used as received without further treatment.

Preparation of silver molybdate: A 0.2 M $AgNO_3$ solution (10 mL) was mixed with a 0.1 M Na_2MoO_4 solution (10 mL) under vigorous magnetic stirring at room temperature. The pH of the mixed solution was adjusted to 1, 5, and 8 by adding dilute HCl or NaOH solution. White precipitates were generated promptly. The resulting suspensions were transferred into Teflon-lined stainless-steel autoclaves without any pretreatment, which were heated at 180 °C for 6 h under microwave radiation; this lead to the precipitation of silver molybdate. After being cooled to room temperature, the products were filtered, washed several times with distilled water until the pH of the washing solution was about 7, and then dried in air at 80 °C for 8 h.

AgCl was synthesized by the ion-exchange reaction between silver molybdate and concentrated HCl with sonication until completion of the ion-exchange process. The AgCl precipitate was collected, washed with deionized water, and dried in air.

The AgCl powder was put into a solution of MO dye, which was then irradiated with a 300 W Xe arc lamp equipped with an ultraviolet cut-off filter to provide visible light with $\lambda \geq 400$ nm. Then the resulting precipitates, which consist of silver NPs and AgCl particles, were washed and dried in air.

The crystal structures of the Ag@AgCl samples were examined by XRD (Bruker AXS D8), their morphology was analyzed by SEM (Hitachi S-4800 microscopy), and their diffuse reflectance was analyzed by UV/Vis spectroscopy (UV-2550, Shimadzu). The content of Ag element in the Ag@AgCl photocatalysts was confirmed by XPS measurements (VG MicroTech ESCA 3000 X-ray photoelectron spectroscope using monochromatic $A1_{K\alpha}$ with a photon energy of 1486.6 eV at a pressure of $>1\times10^{-9}$ torr, a pass energy of 40 eV, an electron take-off angle of 60 °C, and an overall resolution of 0.05 eV). The XPS spectra were fitted using a combined polynomial and Shirley-type background function. A reference photocatalyst, N-doped TiO_2, was prepared by nitridation of commercially available TiO_2 powder (with a surface area of 50 m^2 g) at 773 K for 10 h under a flow of NH_3 (flow rate of 350 mL min^{-1}).[24] The activities of the photocatalysts were evaluated by studying the degradation of methyl orange (MO) dye. The photocatalytic degradation of the MO dye was carried out with the powdered photocatalyst (0.2 g) suspended in a solution (100 mL) of MO dye (20 mg L^{-1}). The optical system for detecting the catalytic reaction included a 300 W Xe arc lamp (PLS-SXE300, Beijing Trusttech Co. Ltd) with a UV cut-off filter (providing visible light $\lambda \geq 400$ nm). The degradation of the MO dye was monitored by UV/Vis spectroscopy (UV-7502PC, Xinmao, Shanghai).

Acknowledgements

This work was financially supported by the National Basic Research Program of China (973 Program, grant 2007CB613302), the National Natural Science Foundation of China (grants 50721002, 10774091, and 20973102).

[1] a) Y. Cui, C. M. Lieber, *Science* **2001**, *291*, 851; b) Y. Xia, P. Yang, Y. Sun, Y. Wu, B. Mayers, B. Gates, Y. Yin, F. Kim, H. Yan, *Adv. Mater.* **2003**, *15*, 353; c) G. R. Patzke, F. Krumeich, R. Nesper, *Angew. Chem.* **2002**, *114*, 2554; *Angew. Chem. Int. Ed.* **2002**, *41*, 2446; d) Y. Q. Zhang, P. L. Chen, L. Jiang, W. P. Hu, M. H. Liu, *J. Am. Chem. Soc.* **2009**, *131*, 2756.

[2] a) S. J. Hurst, E. K. Payne, L. D. Qin, C. A. Mirkin, *Angew. Chem.* **2006**, *118*, 2738; *Angew. Chem. Int. Ed.* **2006**, *45*, 2672; b) M. H. Huang, S. Mao, H. Feick, H. Q. Yan, Y. Y. Wu, H. Kind, E. Weber, R. Russo, P. D. Yang, *Science* **2001**, *292*, 1897; c) E. M. Larsson, J. Alegret, M. Käll, D. S. Sutherland, *Nano Lett.* **2007**, *7*, 1256; d) M. A. El-Sayed, *Acc. Chem. Res.* **2001**, *34*, 257; e) A. K. Boal, F. Ilhan, J. E. DeRouchey, T. Thurn-Albrecht, T. P. Russell, V. M. Rotello, *Nature* **2000**, *404*, 746.

[3] a) K. D. Hermanson, S. O. Lumsdon, J. P. Williams, E. W. Kaler, O. D. Velev, *Science* **2001**, *294*, 1082; b) J. H. Pan, X. W. Zhang, A. J. Du, D. D. Sun, J. O. Leckie, *J. Am. Chem. Soc.* **2008**, *130*, 11256; c) H. B. Zeng, W. P. Cai, P. S. Liu, X. X. Xu, H. J. Zhou, C. Klingshirn, H. Kalt, *ACS Nano* **2008**, *2*, 1661; d) A. P. Alivisatos, *Science* **1996**, *271*, 933.

[4] a) X. C. Wang, X. F. Chen, A. Thomas, X. Z. Fu, M. Antonietti, *Adv. Mater.* **2009**, *21*, 1609; b) M. Engel, J. P. Small, M. Steiner, M. Freitag, A. A. Green, M. C. Hersam, P. Avouris, *ACS Nano* **2008**, *2*, 2425; c) A. M. Yu, G. Q. M. Lu, J. Drennan, I. R. Gentle, *Adv. Funct. Mater.* **2007**, *17*, 2600; d) J. M. Macak, M. Zlamal, J. Krysa, P. Schmuki, *Small* **2007**, *3*, 300; e) D. F. Wang, Z. G. Zou, J. H. Ye, *Chem. Mater.* **2005**, *17*, 3255.

[5] a) K. Maeda, K. Teramura, D. L. Lu, T. Takata, N. Saito, Y. Inoue, K. Domen, *Nature* **2006**, *440*, 295; b) J. G. Yu, F. R. F. Fan, S. Pan, V. M. Lynch, K. M. Omer, A. J. Bard, *J. Am. Chem. Soc.* **2008**, *130*, 7196; c) L. X. Mu, W. S. Shi, J. C. Chang, S. T. Lee, *Nano Lett.* **2008**, *8*, 104; d) H. Uehara, M. Kakiage, M. Sekiya, D. Sakuma, T. Yamonobe, N. Takano, A. Barraud, E. Meurville, P. Ryser, *ACS Nano*, **2009**, *3*, 924; e) J. G. Yu, Y. R. Su, B. Cheng, *Adv. Funct. Mater.* **2007**, *17*, 1984.

[6] a) M. Elvington, J. Brown, S. M. Arachchige, K. J. Brewer, *J. Am. Chem. Soc.* **2007**, *129*, 10644; b) E. Martínez-Ferrero, Y. Sakatani, C. Boissière, D. Grosso, A. Fuertes, J. Fraxedas, C. Sanchez, *Adv. Funct. Mater.* **2007**, *17*, 3348; c) Y. J. Song, R. M. Garcia, R. M. Dorin, H. R. Wang, Y. Qiu, J. A. Shelnutt, *Angew. Chem.* **2006**, *118*, 8306; *Angew. Chem. Int. Ed.* **2006**. *45*, 8126; d) H. R. Wang, Y. J. Song, Z. C. Wang, C. J. Medforth, J. E. Miller, L. Evans, P. Li, J. A. Shelnutt, *Chem. Mater.* **2008**, *20*, 7434; e) S. M. Sun, W. Z. Wang, H. L. Xu, L. Zhou, M. Shang, L. Zhang, *J. Phys. Chem. C* **2008**, *112*, 17835.

[7] a) X. C. Wang, K. Maeda, A. Thomas, K. Takanabe, G. Xin, J. M. Carlsson, K. Domen, M. Antonietti1, *Nat. Mater.* **2009**, *8*, 76; b) G. H. Lu, L. E. Ocola, J. H. Chen, *Adv. Mater.* **2009**, *21*, 1; c) J. H. Kou, Z. S. Li, Y. P. Yuan, H. T. Zhang, Y. Wang, Z. G. Zou, *Environ. Sci. Technol.* **2009**, *43*, 2919; d) Y. J. Song, R. M. Dorin, R. M. Garcia, Y. B. Jiang, H. R. Wang, P. Li, Y. Qiu, F. V. Swol, J. E. Miller, J. A. Shelnutt, *J. Am. Chem. Soc.* **2008**, *130*, 12602; e) M. Higashi, R. Abe, T. Takata, K. Domen, *Chem. Mater.* **2009**, *21*, 1543.

[8] a) C. F. Wu, B. Bull, K. Christensen, Jason McNeill, *Angew. Chem.* **2009**, *121*, 2779; *Angew. Chem. Int. Ed.* **2009**. *48*, 2741; b) X. C. Wang, K. Maeda, X. F. Chen, K. Takanabe, K. Domen, Y. D. Hou, X. Z. Fu, M. Antonietti, *J. Am. Chem. Soc.* **2009**, *131*, 1680; c) J. Xu, W. X. Zhang, Z. H. Yang, S. X. Ding, Ch. Y. Zeng, L. L. Chen, Q. Wang, S. H. Yang, *Adv. Funct. Mater.* **2009**, *19*, 1759; d) Q. Li, R. C. X ie, Y. W. Li, E. Mintz, J. K. Shang, *Environ. Sci. Technol.* **2007**, *41*, 5050.

[9] a) A. Datta, S. Gorai, S. K. Panda, S. Chaudhuri, *Cryst. Growth Des.* **2006**, *6*, 1010; b) J. I. Yamada, H. Akutsu, *Chem. Rev.* **2004**, *104*, 5057; c) J. Reading, M. T. Weller, *J. Mater. Chem.* **2001**, *11*, 2373.

[10] a) M. H. Ge, J. D. Corbett, *Inorg. Chem.* **2007**, *46*, 4138; b) S. S. Mark, M. Bergkvist, X. Yang, L. M. Teixeira, P. Bhatnagar, E. R. Angert, C. A. Batt, *Langmuir* **2006**, *22*, 3763.

[11] Q. Wan, T. H. Wang, *Chem. Commun.* **2005**, *30*, 3841.

[12] J. G. Yu, H. G. Yu, H. T. Guo, M. Li, S. Mann, *Small* **2008**, *4*, 87.

[13] V. Polshettiwar, B. Baruwati, R. S. Varma, *ACS Nano* **2009**, *3*, 728.

[14] D. Chen, J. H. Ye, *Adv. Funct. Mater.* **2008**, *18*, 1922.

[15] L. P. Xu, S. Sithambaram, Y. S. Zhang, C. H. Chen, L. Jin, R. Joesten, S. L. Suib, *Chem. Mater.* **2009**, *21*, 1253.

[16] X. X. Hu, C. Hu, J. H. Qu, *Appl. Catal. B* **2006**, *69*, 17.

[17] C. W. Beier, M. A. Cuevas, R. L. Brutchey, *Small* **2008**, *4*, 2102.

[18] L. W. Zhang, Y. J. Wang, H. Y. Cheng, W. Q. Yao, Y. F. Zhu, *Adv. Mater.* **2009**, *21*, 1286.

[19] a) S. L. Xiong, B. J. Xi, C. M. Wang, D. C. Xu, X. M. Feng, Z. C. Zhu, Y. T. Qian, *Adv. Funct. Mater.* **2007**, *17*, 2728; b) P. Wang, B. B. Huang, X. Y. Zhang, X. Y. Qin, Y. Dai, H. Jin, J. Y. Wei, M.-H. Whangbo, *Chem. Eur. J.* **2008**, *14*, 10543.

[20] a) X. Chen, H. Y. Zhu, J. C. Zhao, Z. F. Zheng, X. P. Gao, *Angew. Chem.* **2008**, *120*, 5433; *Angew. Chem. Int. Ed.* **2008**, *47*, 5353; b) P. Wang, B. B. Huang, X. Y. Zhang, X. Y. Qin, H. Jin, Y. Dai, Z. Y. Wang, J. Y. Wei, J. Zhan, S. Y. Wang, J. P. Wang, M.-H. Whangbo, *Chem. Eur. J.* **2009**, *15*, 1821.

[21] P. Wang, B. B. Huang, X. Y. Qin, X. Y. Zhang, Y. Dai, J. Y. Wei, M.-H. Whangbo, *Angew. Chem.* **2008**, *120*, 8049; *Angew. Chem. Int. Ed.* **2008**, *47*, 7931.

[22] H. Zhang, G. Wang, D. Chen, X. J. Lv, J. H. Li, *Chem. Mater.* **2008**, *20*, 6543.

[23] M. R. Hoffmann, S. T. Martin, W. Choi, W. Bahnemann, *Chem. Rev.* **1995**, *95*, 69.

[24] K. Maeda, Y. Shimodaira, B. Lee, K. Teramura, D. Lu, H. Kobayashi, K. Domen, *J. Phys. Chem. C* **2007**, *111*, 18264.

Received: July 15, 2009
Published online: November 13, 2009

